Journal of Engineering and Technology for Industrial Applications

ISSN ONLINE: 2447-0228

ITEGAM-JETIA

Manaus, v.12 n.58, p.1417-1426. March/April, 2026.
DOI: https://doi.org/10.5935/jetia.v12i58.3364

RESEARCH ARTICLE OPEN ACCESS

INTELLIGENT TECHNIQUE FOR ELECTROMECHANICAL SYSTEM DATA BY USING MODEL OF NARX NEURAL NETWORK

Mohammed Al-Abbasi*[1], Tamarah Kareem[2]

[1, 2]Electro-Mechanical Engineering Department, University of Technology-Iraq.

[1]https://orcid.org/0000-0001-8985-4958, [2]https://orcid.org/0000-0002-0994-584X

Email: *Mohammed.S.Dawood@uotechnology.edu.iq, Tamarah.A.Kareem@uotechnology.edu.iq,

ARTICLE INFO

Article History
Received: January 20, 2026
Reviewed: February 24, 2026
Accepted: April 3, 2026
Published: April 30, 2026

Keywords:
Artificial Intelligence,
Vibration,
Narx Neural Network,
Electromechanical Systems,
Accelerometer Sensor.

ABSTRACT

In this study, the electromechanical systems have been modeled using the neural network technique. One of the most important parts of engineering is system modeling, which is essential for both system analysis and control process implementation, especially when a sophisticated and accurate modeling approach like NARX neural networks is employed. In order to gather the vibration produced by the electromechanical system devices after a sinusoidal voltage between zero and forty volts was applied, a practical test was carried out in this study. One side of the actuator was fixed, while the other side was free. After double integration for the output signal, the displacement data was gathered using an accelerometer sensor. Following variable modification, the transfer function, which shows the system's dynamic behavior based on input and output data is produced. NARX neural network approach was utilized for modeling using the MATLAB application. The outcomes demonstrated how well the NARX neural network approach represented the system and produced an appropriate transfer function in the time and frequency domains. Prior to and throughout the modeling process, the system's behavior remained unchanged, and the minimal mean square error was 0.00001391.

I. INTRODUCTION

The unique electromagnetic characteristics of piezoelectric materials allow them to transform electrical to kinetic energy and transform kinetic to electrical energy. Piezoelectric materials are usually used as sensors or actuators [1], [2]. Researchers are interested in this material for a variety of uses, such as bioengineering, robotics, and micro- and nano-instruments [3-5]. J.W.Curie discovered the piezoelectric impact in 1880 when he created an electric charge by applying mechanical stress [6]. One of the most challenging parts of modeling piezoelectric actuators is their physical properties, which are influenced by thermal and electrical elements, such as frequency and temperature [7], [8]. particularly those involving non-linear conduct and high-stress deformations that impact the electrical or mechanical response [9].

Finally, resonance, undesired vibrations, and hysteresis are ways in which actuators may respond to the electrical, mechanical, or electronic systems in their immediate surroundings [10]. Modeling may become more difficult due to the aforementioned circumstances, necessitating the development of an accurate model using innovative techniques to guarantee consistent and dependable performance [11]. Depending on their intended function, a number of researchers have employed piezoelectrics as sensors and actuators. "Piezoelectric effect" or the ability of some materials to generate an electric charge when subjected to mechanical stress, as seen in Figure 1. The "inverse effect" is the "piezoelectric effect" in reverse [12].

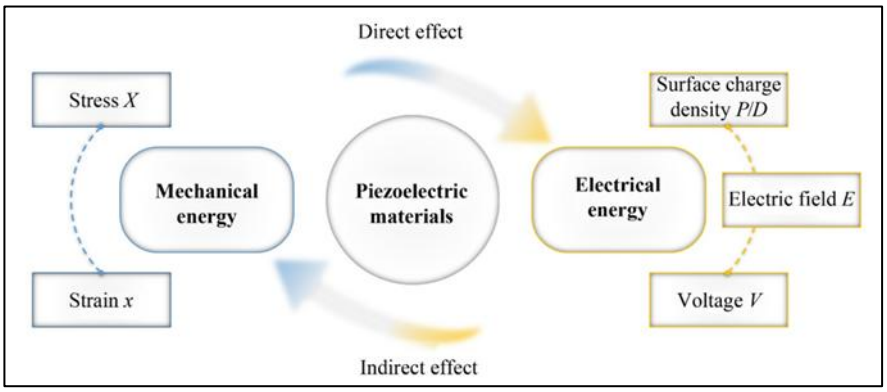

Figure 1: Piezoelectric effect energy conversion.
Source: Authors, (2026).

The piezoelectric effect is frequently caused by the electromechanical interaction between the characteristics of the elastic and the dielectric. While dielectric characteristics primarily relate to the interaction between electric field and electrical displacement, elastic characteristics are related to the link between stress and strain. Understanding both traits is essential to understanding a material's behavior [12-14]. The two main types of piezoelectric actuators (PZA) are direct and indirect actuators. Piezoelectric actuators that use the stretching action of the piezoelectric film in a straightforward manner without requiring a complex structural and primary design are known as direct piezoelectric actuators.

As a result, it combines attributes like high accuracy, simple design, and quick reaction [15], [16] and it is particularly useful for applications that call for rapid strokes and incredibly high precision. Unlike direct piezoelectric actuators, indirect piezoelectric actuators use complex structures to convert piezoelectric material deformation into indirect displacement. There is more to the link between material deformation and output displacement than just amplification. Stepping and repeating are two methods that indirect piezoelectric actuators can use to produce larger strokes and responses with more degrees of freedom (DOFs) [16-18]. However, the outcome might be more complexity and worse resolution.

This large class consists of two subgroups, one of which is stepping actuators [19]. Moreover, ultrasonic actuators [20], based on the operating concept. Piezoelectric modeling has received a lot of attention lately since it is essential for controlling systems as well as simulating systems, such as sensors or actuators. An imprecise modeling method will lead to unstable signals and inaccurate results [21-31], [8]. Li and associates used a backpropagation neural network and a genetic algorithm to simulate the linear piezoelectric actuator [21]. To model PZA, Shields and Konefat employed a finite element approach [22]. In a number of publications [23], Furthermore, PZA hysteresis is predicted based on various loads [24].

For example, models of composition could not reliably distinguish between the relative stability of inorganic materials [25]. Rather, They discovered that utilizing a CGCNN graph neural network, adding structure to the representation might result in non-incremental increases in stability forecasts, which is a strong argument for structural models. Although there are many ML models for various material properties, there is currently no study on ML prediction of piezoelectric coefficients in the literature. The aim of this work is to create a machine learning (ML) model that can accurately forecast piezoelectric modulus so that new, eco-friendly piezoelectric materials may be screened. A piezoelectric material's volume changes when an electric field or stress is applied to it.

This change is measured by the piezoelectric coefficient, also known as the piezoelectric modulus and often represented as d33 [8], [26-30]. The multi-layer feedforward neural network uses the nonlinear autoregression-moving average exogenous input technique to mimic the dynamics of piezoelectric actuators. The literature describes a neural network hysteresis model with an improved Preisach model to predict a piezoelectric actuator's output [27]. This work's primary contribution is to introduce a novel NARX neural network modeling approach for the PZA. In this study, PZA, the NARX neural network model (NARX NNET), and an experimental effort to gather input and output data using integrated measuring devices and sensors are introduced. The findings are then presented.

II. THEORETICAL REFERENCE

NARX Neural networks may be used in this study to accurately represent piezoelectric actuators in both the time and frequency domains. It identifies how to model piezoelectric actuators and utilize neural networks to achieve high accuracy, thus enabling their widespread application once the model is tested to verify its functionality with the required precision. The time and frequency domains are of particular interest to researchers studying the dynamic behavior of lag, creep, and vibration when data is used in systems such as nano-positioning platforms and atomic force microscopes.

Neural networks can be described as a training and learning modeling technique that relies on experimental procedures for data. Configuration equations are employed to establish the relationships between input and output. The concepts of magnetic lag and creep fall within the realm of nonlinear systems and are time-domains. They can be modeled using neural networks by simulating piezoelectric actuators under various input signal values. One phenomenon requiring study at constant voltage is creep, which exhibits a continuous and slow displacement. Neural networks can be employed by incorporating the time domain as an input feature.

Deviation and displacement correspond to time modeling, while frequency corresponds to vibration on one hand and dynamics on the other. Neural networks can be used to model the electro-efficient response of motor dynamics. Tests can be conducted by setting operating conditions that include the operating range of a frequency signal. Neural networks can be trained to achieve high-precision performance using a nonlinear hybrid prediction system that simulates the dynamics of a spring, block, or damper, according to the requirements of the model being trained.

Previous studies and literature have identified several types of neural networks, including feedforward neural networks (FNNs), multilayer neural networks (MLPs), long-term memory neural networks (LSTMs), recurrent neural networks (RNNs), vector primitive function neural networks (RBFNNs), and a deep neural network called DenseNet. These networks are characterized by high accuracy, adaptability to varying operating conditions, robustness, high performance, and rapid execution after training.

II.1 NARX NEURAL NETWORK MODEL

The NARX network is a recurrent dynamic network that has many network layers enclosed by feedback links. The linear ARX model, which is frequently utilized in time-series modeling, is the foundation of the NARX model [32]. a diagram illustrating the components of cells and layers of a NARX neural network model can be seen, as shown in the figure.

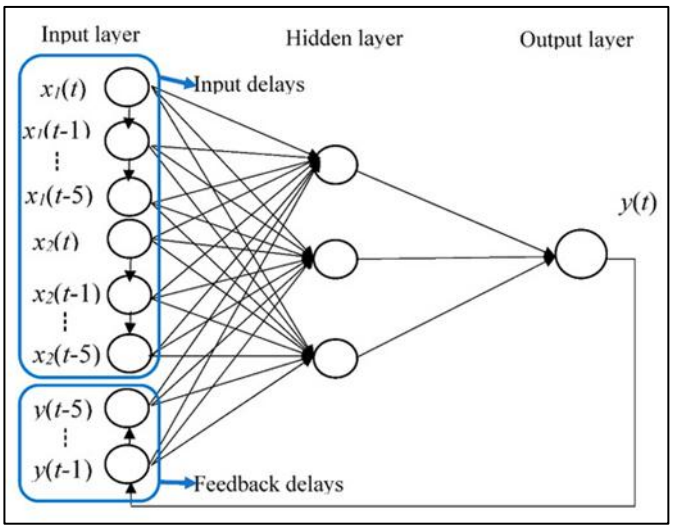

Figure 2: The NARX model's structure.
Source: [32].

The input, hidden, and output layers of the NARX model are made up of connected neurons (Figure1). The input layer, which is made up of the input parameters, permits the data to be received into the network. The data is then passed to the hidden layers for progressive processing, which results in the output layer. As part of the typical NARX design, the output is transmitted back to the feedforward neural network's input. Since runoff is closely correlated with net rainfall and discharge, The input parameters are evapotranspiration and precipitation. The NARX model's defining equation is as follows:

$$y(t) = f\,[y\,(t-1), y\,(t-2), \ldots . y\,(t-m), \mu\,(t-1), \mu\,(t-2), \ldots . \mu\,(t-n)] \quad (1)$$

The process of evapotranspiration E(t),E(t - 1),...E(t - 5), precipitation P(t),P(t - 1),...P(t - 5), and discharge Q(t - 1),Q(t - 2),...Q(t - 5) were chosen as input parameters following rigorous evaluation of the model input components and surface runoff routing time. The anticipated discharge Q(t) served as a representation of the output.. The NARX model chooses a sigmoidal activation function for the hidden layer, which helps speed up ANN training. The Arithmetical Mean Method was used to calculate the average value of input data over a catchment (Rakhecha and Singh, 2009) [33]. Trial and error methods were used to determine the number of concealed nodes. The empirical formula provided by [32]. was used to calculate the number of hidden neurons.

To improve the accuracy of the input to the feedforward network, series-parallel designs are developed for the output layer that use the actual output rather than feeding back the anticipated output. The algorithm of Levenberg-Marquardt, which blends the benefits of the gradient descent method with the Gauss-Newton algorithm, may be used to optimize the NARX model. The maximum number of epochs is set at 1000, and the error gradient and Levenberg-Marquardt correction variables are set at 10−7 and 10−10, respectively. The NARX procedure is terminated if one of the aforementioned criteria meets the objectives. Further information is available in [34]. The following formula is used to determine the output variable:

$$Y_I = f \sum_{K=1}^{N} x_k w_{k,i} + b_i \quad (2)$$

Y is the output variable in this case, N is the number of nodes in the preceding layer, w is the weight, b is the bias, and x is the hidden layer data. Three sections were created using the observation's precipitation, evapotranspiration, and discharge data: 62.5% of the 2922 time series were selected at random for training, 12.5% for verification, and 25% for testing. In other words, training samples from 2001 to 2005, validation samples from 2006, and test samples from 2007 to 2008. Considering how extreme values affect the training network and the faster convergence, Prior to trainingnormalized the input data to fall between 0 and 1, and following training, they were resized to their initial values. The network model's simulation results are significantly impacted by the NARX structure's main parameter.

Two input variables, one hidden layer, ten hidden neurons, five-day delays, and one output target were used in this study to determine the best architecture of the NARX model based on the previously examined and trained data. The mean square error is used to assess the NARX model's performance.

II.2 MODEL STRUCTURE

Voltage and frequency are the two inputs of the suggested NNET model for PEA's nonlinear behavior. One output is the displacement. In order to minimize the total of the mean squared error, we employed a multi-layer feed-forward backpropagation neural network with the Levenberg-Marquardt algorithm. The equation provides the Levenberg-Marquardt algorithm, which is based on the steepest descent and Newton algorithms. Ten fully linked hidden layers make up the NNET model. For both the ANN output layer and each input layer, the so-called logistic activation function was employed [35].

$$f(n) = \frac{1}{1 + exp^{-n}} \tag{3}$$

II.3 MODEL OF SYSTEM IDENTIFICATION

After combining and multiplying the inputs to a neuron by their individual weights, the first step in neural computing is to add a bias term. This procedure is known as the weighted sum or linear combination. Regularization parameters can be used to determine the optimal hyperplane, or activation function, in a quadratic programming issue. Many widely utilized and well-liked activation functions, such as "Tanh," "Sigmoid," "Softplus," "Swish," "Arctan," "ReLU" and "Mish" [28], [29], may be used because the desired solutions do not need to be regular. It is expressed mathematically as equations.

The linear kernel: $$K(x,y) = x \times y \tag{4}$$

The polynomial kernel: $$K(x,y) = [(x \times y) + 1]^d \tag{5}$$

The Sigmoid kernel: $$K(x,y) = tanh\,(\beta_0\, x\, y + \beta_1) \tag{6}$$

RBF kernel: $$K(x,y) = exp(-\gamma\,||x - y||)^2 \tag{7}$$

It will be possible to determine the parameters d, β_0, β_1, and γ experimentally.

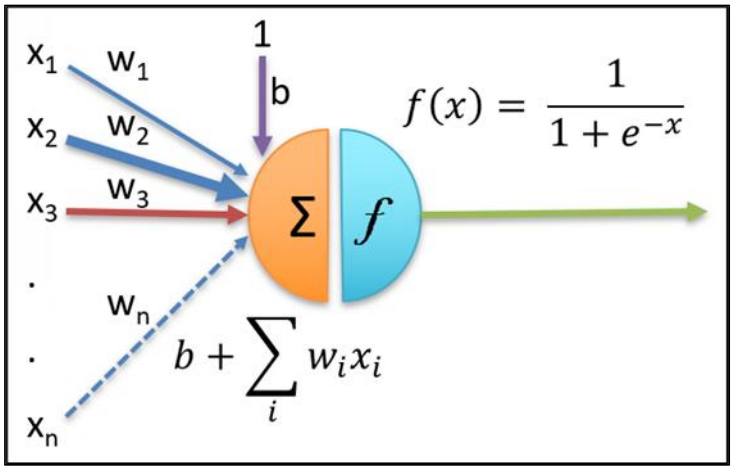

Figure 3: Display the neural network's mathematical architecture.
Source: Authors, (2026).

II.4 INTEGRATED GADGETS AND EXPERIMENTAL RIGS

The PZT system was developed to replicate the dynamic behavior system by collecting input and output data. PZT type QDA40-20-0.7, which had dimensions of 40 mm in length, 20 mm in breadth, and 0.7 mm in thickness, was the first of the system's five components. The boost DC-DC power converter module type XL 6009 boosted the voltage to 40 V. The second component was a plexiglass holder that held the PZT in place. Its dimensions were 150 mm for length, 100 mm for breadth, and 10 mm for thickness. As seen in Figures 2 and 3, the holder is made up of three layers. The first layer served as the foundation for the construction, while the other two layers were used for PZT fixation and were joined by four screws.

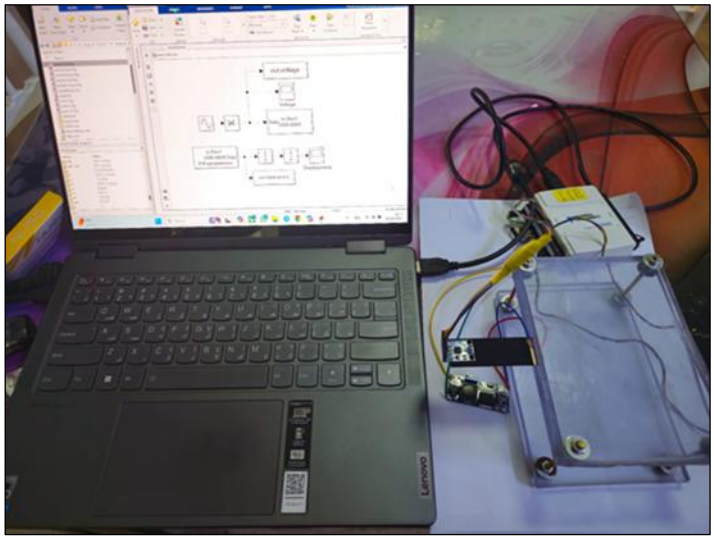

Figure 4: PZT test apparatus.
Source: Authors, (2026).

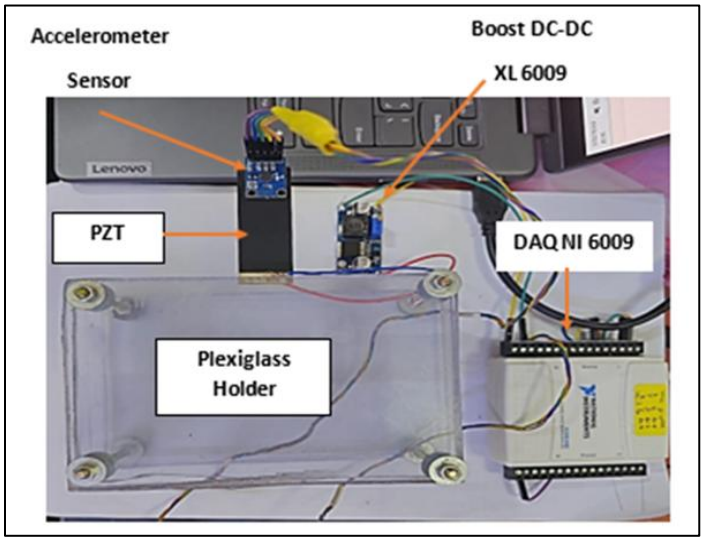

Figure 5: Components of the PZT System.
Source: Authors, (2026).

The third part was an NI USB-6009 USB data collection system (DAQ), which included four digital input ports, eight digital output ports, two analog output ports, and eight analog input ports. The ADXL335 accelerometer sensor, which gathers acceleration from PZT, was the fourth component. As seen in Figure 4, finally A computer running MATLAB 2024b was used as a component to send the signal to PZT, improve it, and collect displacements in real-time using an accelerometer.

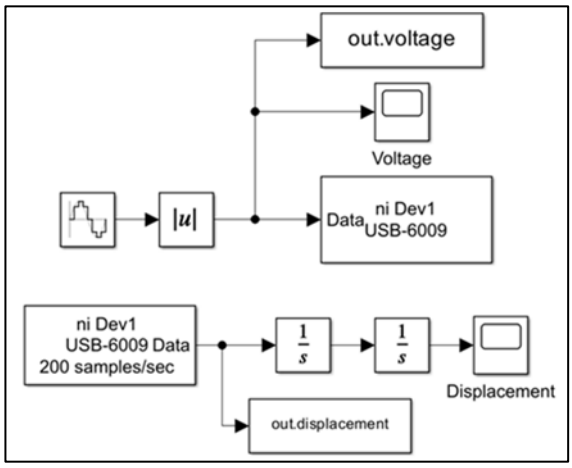

Figure 6: Real-Time System Simulink in MATLAB.
Source: Authors, (2026).

III. DISCUSSIONS OF RESULTS

This work used the NARX NNET model to represent the electromechanical PZT system by collecting input data as a voltage and output data as a displacement using double integration. The work is managed in real time using the MATALB application 2024b. As seen in Figures 7 and 8, 200 data points were gathered in seconds to 10 seconds for the output..

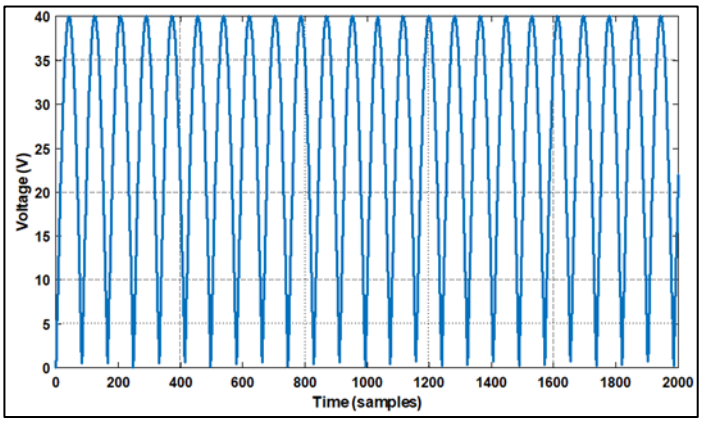

Figure 7: The voltage that PZT receives.
Source: Authors, (2026).

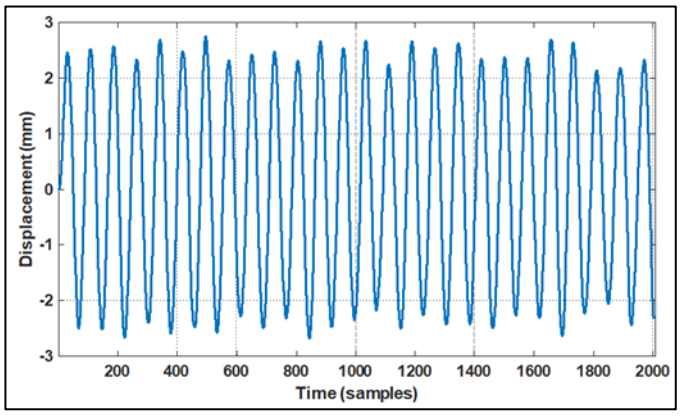

Figure 8. Data on displacement for PZT.
Source: Authors, (2026).

NARX NNET is used to model the PZT in order to determine the optimal solution and produce the final transfer function. Using a validation set of 25% and a testing set of 25%, 50% of the data was used for training. The findings displayed in Table 1 were then obtained by changing the number of hidden neurons (Nn) from 1 to 10 and setting the number of delays (Nd) to 2.

Table 1 : Nd was set to 2 by training and assessing the impacts of error.

Case 1					
Number of Hidden Neurons	**Number of Delay**	**Mean Square Error Training**	**Mean Square Error Valdation**	**Mean Square Error Testing**	**Mean Square Error**
1	2	$1.37577*10^{-5}$	$1.41543*10^{-5}$	$2.35120*10^{-5}$	$1.7615*10^{-5}$
2	2	$1.65984*10^{-5}$	$1.31694*10^{-5}$	$1.42830*10^{-5}$	$1.6439*10^{-5}$
3	2	$1.12691*10^{-5}$	$1.23777*10^{-5}$	$2.25385*10^{-5}$	$1.5351*10^{-5}$
4	2	$1.63333*10^{-5}$	$1.12396*10^{-5}$	$1.20918*10^{-5}$	$1.5624*10^{-5}$
5	2	$1.24028*10^{-5}$	$1.07687*10^{-5}$	$2.11209*10^{-5}$	$1.5854*10^{-5}$
6	2	$1.11409*10^{-5}$	$1.12074*10^{-5}$	$2.02379*10^{-5}$	$1.4756*10^{-5}$
7	2	$1.12874*10^{-5}$	$1.07001*10^{-5}$	$2.34641*10^{-5}$	$1.5688*10^{-5}$
8	2	$1.36204*10^{-5}$	$1.05382*10^{-5}$	$1.29142*10^{-5}$	$1.4295*10^{-5}$
9	2	$1.06392*10^{-5}$	$8.63022*10^{-6}$	$1.88759*10^{-5}$	$1.4375*10^{-5}$
10	2	$1.35594*10^{-5}$	$9.97823*10^{-6}$	$1.41160*10^{-5}$	$1.7139*10^{-5}$

Source: Authors, (2026).

Based on the data shown in Table 1, At Nn = 8 and Nd = 2, the mean square error (MSE) with the lowest value was found to be 0.000014295. As indicated in table 2, To find the lowest error rate for the behavior of the system, Nd was changed from 1 to 10 and Nn was kept at 8.

Table 2: Nn was set to 8 by training and assessing the impacts of error.

Case 2					
Number of Hidden Neurons	**Number of Delay**	**Mean Square Error Training**	**Mean Square Error Valdation**	**Mean Square Error Testing**	**Mean Square Error**
8	1	$1.95686*10^{-2}$	$2.12564*10^{-2}$	$1.93901*10^{-2}$	0.0199
8	2	$1.52031*10^{-5}$	$1.09815*10^{-5}$	$1.10995*10^{-5}$	$1.4563*10^{-5}$
8	3	$5.65258*10^{-6}$	$1.24688*10^{-5}$	$1.49241*10^{-5}$	$2.9307*10^{-4}$
8	4	$6.14545*10^{-6}$	$1.41665*10^{-5}$	$4.36092*10^{-6}$	$3.0608*10^{-4}$
8	5	$3.77136*10^{-6}$	$1.34972*10^{-5}$	$4.94665*10^{-6}$	$1.6749*10^{-5}$
8	6	$8.26632*10^{-6}$	$1.44869*10^{-5}$	$4.18769*10^{-6}$	$1.3910*10^{-5}$
8	7	$3.97473*10^{-7}$	$5.00190*10^{-7}$	$7.81449*10^{-5}$	$6.0951*10^{-5}$
8	8	$3.08907*10^{-7}$	$4.10183*10^{-7}$	$7.99605*10^{-5}$	$7.2211*10^{-5}$
8	9	$3.50602*10^{-6}$	$2.08055*10^{-5}$	$1.21688*10^{-5}$	$1.5616*10^{-5}$
8	10	$3.08372*10^{-6}$	$1.17104*10^{-5}$	$2.93209*10^{-6}$	$1.7256*10^{-5}$

Source: Authors, (2026).

According to Table 2, the system's smallest MSE is 0.0001391 at Nn 8 and Nd 6. As a result, the system's optimal block diagram, depicted in Figure 9, was found.

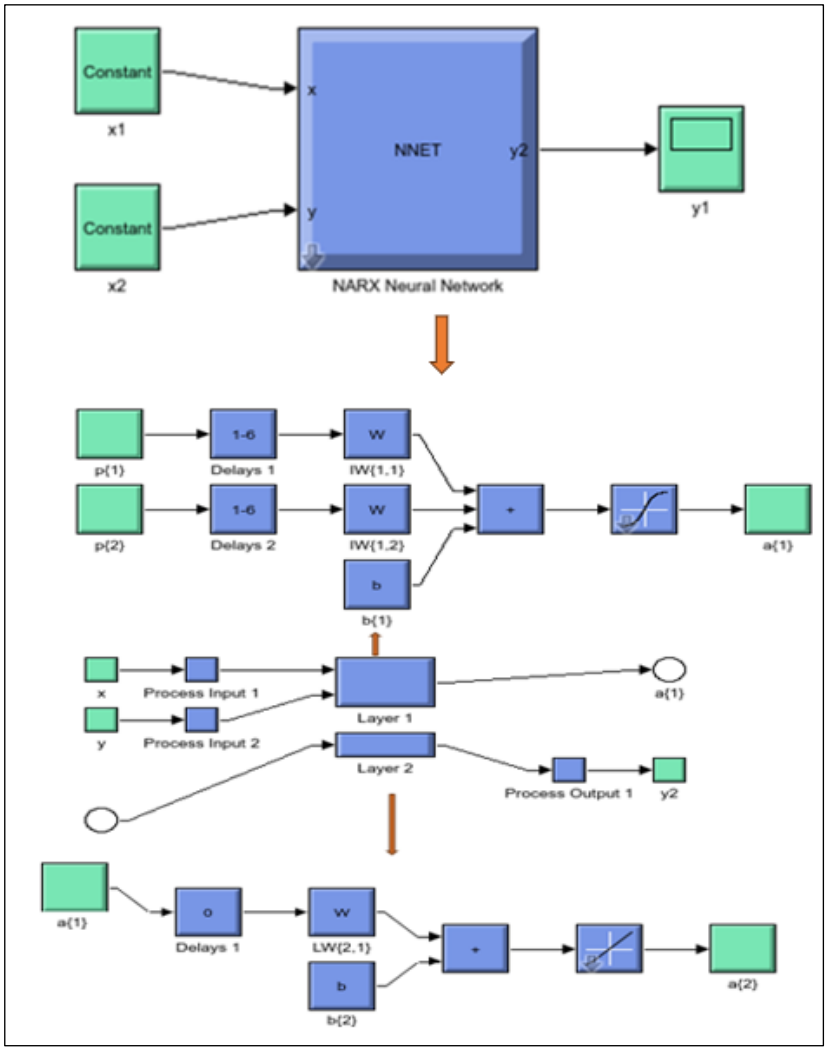

Figure 9: Block diagram for NARX NNET Simulink in MATLAB.
Source: Authors, (2026).

10001 data were utilized for training, and the remaining 1000 data were used to assess the performance of the prediction system. Every attempt was verified using the MSE approach to determine the optimal system performance and produce the final transfer function. Figure 11 displays the error between the real and projected data, whereas Figure 10 demonstrates that the NARX NNET approach was successful in forecasting the system behavior with the lowest MSE up to 0.0001391.

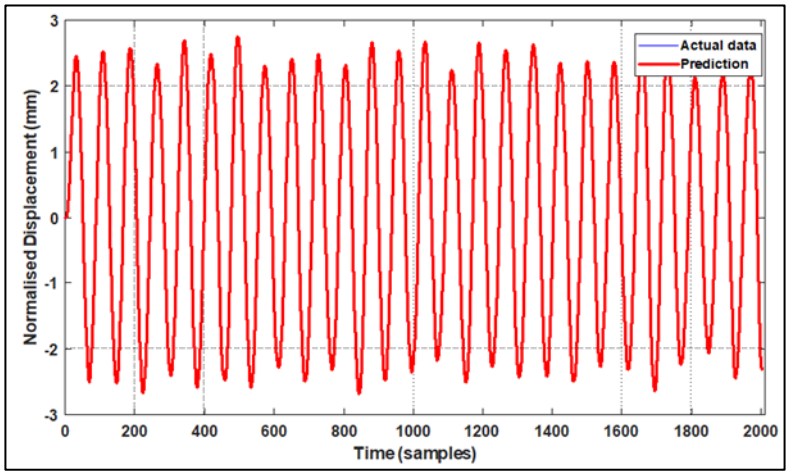

Figure 10: Normalized Displacement Data: Actual and Predicted.
Source: Authors, (2026).

The graph is an excellent representation of the performance of a predictive model comparing the actual and observed behavior of a dynamic system (standard displacement) over time. Both lines (blue and red) show consistent periodic oscillatory behavior across the entire time axis. The most striking observation is the near-perfect match between the actual data and the predictions.

The red line overlaps the blue line almost perfectly. The predictive model accurately captures the amplitude of the oscillations, which ranges from approximately -2.5 mm to +2.5 mm, and also tracks the frequency perfectly.

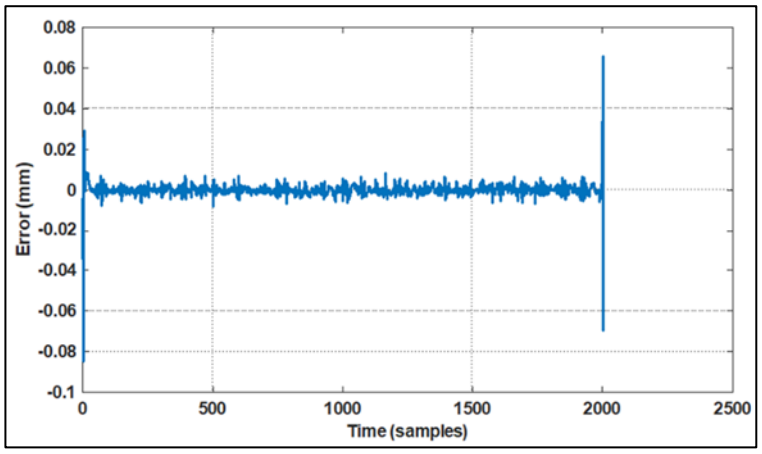

Figure 11: Actual and predicted output data error.
Source: Authors, (2026).

A control or measuring system (Figure 11) system's steady-state random error and abrupt disruption behavior over time are depicted in the diagram. The diagram shows that the system is sensitive to a huge, localized disruption that occurs at a particular moment in time, but it also shows that the system maintains a precise and regulated steady-state. To determine the underlying reason of this abrupt surge, it is necessary to comprehend the unique operating environment of the system.

Table 3: A comparison of the techniques employed in earlier investigations with MSE is presented.

REF	METHOD	MES
[36]	NARX neural networks	0.0858
[36]	LSTM neural networks	0.0279
[37]	Levenberg–Marquardt method (LMM-NNs)	6.7^{-6}
[37]	Bayesian Regularization method (BRM-NNs)	8.6^{-11}
[38]	OCNN-Hammerstein model	0.45^{-6}
[39]	K-NARXNN	0.0114
Proposed model	NARX NNET	0.0001391

Source: Authors, (2026).

IV. CONCLUSIONS

For the electromechanical system device, the potential of feedforward networks' multi-layered architecture—that is, NARX NNET backpropagation neural networks—was utilized to provide accurate, outstanding, and efficient results. We used Narx nnet in MATLAB to apply the suggested technique, and we were able to get the most accurate findings for a performance study utilizing regression and squared error analyses. The results showed that the Narx NNET technique achieved high modeling precision in both the frequency and time domains, with a low mean square error (MSE) of 0.0001391. The model's accuracy and stability were validated using the Narx NNET, and a correlation test showed that the measured output and the model output closely matched. These findings show how well the Narx NNET approach generates accurate dynamic system models, this makes it an effective tool for designing control systems and analyzing electromechanical system devices.

V. AUTHOR'S CONTRIBUTION

Conceptualization: Mohammed Al-Abbasi and Tamarah Kareem.
Methodology: Mohammed Al-Abbasi.
Investigation: Mohammed Al-Abbasi and Tamarah Kareem.
Discussion of results: Mohammed Al-Abbasi and Tamarah Kareem.
Writing – Original Draft: Mohammed Al-Abbasi.
Writing – Review and Editing: Mohammed Al-Abbasi.
Resources: Tamarah Kareem.
Supervision: Mohammed Al-Abbasi and Tamarah Kareem.
Approval of the final text: Mohammed Al-Abbasi.

VI. ACKNOWLEDGMENTS

Write a word of thanks to those who contributed to this research but are not listed in the authors' bibliography. Acknowledgments: To the University of Technology/College of Electromechanical Engineering and College of Computer Science, Baghdad/Iraq.

VII. REFERENCES

[1] Ferreira PM, Machado MA, Carvalho MS, Vidal C. Embedded sensors for structural health monitoring: methodologies and applications review. Sensors 2022;22. https://doi.org/10.3390/s22218320.

[2] He, L.; Yue, X.; Dou, H.; Ge, X.; Wan, Z.; Qian, A. Research on variable stiffness asymmetrical resonant linear piezoelectric actuator based on multi-modal drive. Smart Mater. Struct. 2024, 33, 015032.

[3] Guan, J., Deng, J., Zhang, S., Liu, J., & Liu, Y. (2024). A spatial 3-DOF piezoelectric robot and its speed-up trajectory based on improved stick-slip principle. Sensors and Actuators A: Physical, 374, 115502.

[4] Xue, H., Jin, J., Tan, Z., Chen, K., Lu, G., Zeng, Y., ... & Wu, J. (2024). Flexible, biodegradable ultrasonic wireless electrotherapy device based on highly self-aligned piezoelectric biofilms. Science Advances, 10(22), eadn0260.

[5] Yuan, Z., Zhou, S., Zhang, Z., Xiao, Z., Hong, C., Chen, X., ... & Li, X. (2024). Piezo-actuated smart mechatronic systems: Nonlinear modeling, identification, and control. Mechanical Systems and Signal Processing, 221, 111715.

[6] S.B. Lang, S. Muensit, Review of some lesser-known applications of piezoelectric and pyroelectric polymers, Appl. Phys. A 85 (2006) 125e134.

[7] Gao, X., Yang, J., Wu, J., Xin, X., Li, Z., Yuan, X., ... & Dong, S. (2020). Piezoelectric actuators and motors: materials, designs, and applications. Advanced Materials Technologies, 5(1), 1900716.

[8] Mohammed, M. J., & Kareem, T. A. (2025). Vibration Performance on the 3D-Printed UAV Wing. Journal Européen des Systèmes Automatisés, 58(4), 815.

[9] Kanchan, M., Santhya, M., Bhat, R., & Naik, N. (2023). Application of modeling and control approaches of piezoelectric actuators: a review. Technologies, 11(6), 155.

[10] Febbo, M., Machado, S. P., Oliva, A., Ortiz, M., & Pereyra, N. (2023). Modelling of a piezoelectric beam with a full-bridge rectifier under arbitrary excitation: experimental validation. Energy Harvesting and Systems, 10(2), 311-324.

[11] Gan, J., & Zhang, X. (2019). A review of nonlinear hysteresis modeling and control of piezoelectric actuators. AIP Advances, 9(4).

[12] Zhou, X., Wu, S., Wang, X., Wang, Z., Zhu, Q., Sun, J., ... & Lu, Q. (2024). Review on piezoelectric actuators: materials, classifications, applications, and recent trends. Frontiers of Mechanical Engineering, 19(1), 6.

[13] Momin, R. T. (2023). Piezoelectric Sensors for Real-time Monitoring and Quality Control in Additive Manufacturing. arXiv preprint arXiv:2310.14321.

[14] Chen, Zhihao, et al. "Microstructure-property relationships in piezoelectric-polymer composites: a review." Journal of Polymer Research 32.2 (2025): 41.

[15] Wang S P, Rong W, Wang L F, Xie H, Sun L, Mills J K. A survey of piezoelectric actuators with long working stroke in recent years: classifications, principles, connections and distinctions. Mechanical Systems and Signal Processing, 2019, 123: 591–605.

[16] Zhang Z. M, An Q, Li J M, Zhang W J. Piezoelectric friction–inertia actuator—a critical review and future perspective. The International Journal of Advanced Manufacturing Technology, 2012, 62(5–8): 669–685.

[17] Spanner K, Koc B. Piezoelectric motors, an overview. Actuators, 2016, 5(1): 6.

[18] Hunstig M. Piezoelectric inertia motors—a critical review of history, concepts, design, applications, and perspectives. Actuators, 2017, 6(1): 7.

[19] Chen F X, Zhang Q J, Gao Y Z, Dong W. A review on the flexurebased displacement amplification mechanisms. IEEE Access, 2020, 8: 205919–205937.

[20] Tian X Q, Liu Y X, Deng J, Wang L, Chen W S. A review on piezoelectric ultrasonic motors for the past decade: classification, operating principle, performance, and future work perspectives. Sensors and Actuators A: Physical, 2020, 306: 111971.

[21] Li, H., Tong, Y., & Li, C. (2024, January). Modeling and control of a linear piezoelectric actuator. In Actuators (Vol. 13, No. 2, p. 55). MDPI.

[22] Shields, J., & Konefat, E. (2021). Modeling of Piezoceramic. Piezoelectric Actuators: Principles, Design, Experiments and Applications, 81.

[23] Ge, P., & Jouaneh, M. (1995). Modeling hysteresis in piezoceramic actuators. Precision engineering, 17(3), 211-221.

[24] Georgiou, H. M., & Mrad, R. B. (2006). Electromechanical modeling of piezoceramic actuators for dynamic loading a
pplications.

[25] Bartel, Christopher J., et al. "A critical examination of compound stability predictions from machine-learned formation energies." npj computational materials 6.1 (2020): 97.

[26] Hu, Jeffrey, and Yuqi Song. "Piezoelectric modulus prediction using machine learning and graph neural networks." Chemical Physics Letters 791 (2022): 139359.

[27] Wang, Geng, et al. "A novel piezoelectric hysteresis modeling method combining LSTM and NARX neural networks." Modern Physics Letters B 34.28 (2020): 2050306.

[28] Zhang, Peijun, et al. "Boundary integrated neural networks for 2D elastostatic and piezoelectric problems." International Journal of Mechanical Sciences 280 (2024): 109525.

[29] AL-Abbasi, Mohammed, Tamarah Kareem, and Salam Waley Shneen. "Efficient Face Mask Detection Using Hybrid Deep Learning Algorithms." Journal of Qadisiyah Computer Science & Mathematics 16.4 (2024).

[30] Kareem, T., Shneen, S. W., & Al-Abbasi, M. (2025). Design and Implementation of Proportional-Integral Controller for Single Phase Stand-Alone Inverter with an LC-Filter. International Journal of Robotics & Control Systems, 5(2).

[31] Tamarah A Kareem, Mohammed Al-Abbasi and Mayada T Wazi (2024) “Analyzing Boost Converter Circuit by Using State Variables Methodology” SAR Journal (2619-9955).

[32] Shao, Yuehong, et al. "Application of rainfall-runoff simulation based on the NARX dynamic neural network model." Water 14.13 (2022): 2082.

[33] Nonki, Rodric M., et al. "Performance assessment and uncertainty prediction of a daily time-step HBV-Light rainfall-runoff model for the Upper Benue River Basin, Northern Cameroon." Journal of Hydrology: Regional Studies 36 (2021): 100849.

[34] Thapa, S.; Zhao, Z.; Li, B.; Lu, L.; Donglei Fu, D.L.; Xiaofei Shi, X.F.; Tang, B.; Qi, H. Snowmelt-Driven Streamflow Prediction Using Machine Learning Techniques (LSTM, NARX, GPR, and SVR). Water 2020, 12, 1734.

[35] Paralı, Levent, et al. "The artificial neural network modelling of the piezoelectric actuator vibrations using laser displacement sensor." Journal of Electrical Engineering 68.5 (2017): 371.

[36] Wang, Geng, et al. "A novel piezoelectric hysteresis modeling method combining LSTM and NARX neural networks." Modern Physics Letters B 34.28 (2020): 2050306.

[37] Naz, Sidra, et al. "Intelligent predictive solution dynamics for Dahl hysteresis model of piezoelectric actuator." micromachines 13.12 (2022): 2205.

[38] Jin, Jiaxi, Xuan Sun, and Zhaobo Chen. "Inverse feedforward control of piezoelectric actuators using optimized composite neural network-based Hammerstein model." Journal of Intelligent Material Systems and Structures 35.20 (2024): 1558-1575.

[39] Zhu, Binkai, et al. "Hysteresis modeling of piezoelectric actuators based on neural network considering load and environmental stiffness." Journal of Physics: Conference Series. Vol. 2820. No. 1. IOP Publishing, 2024.